Available online at www.sciencedirect.com

SCIENCE DIRECT®

Earth and Planetary Science Letters 233 (2005) 71–86

EPSL

www.elsevier.com/locate/epsl

A high-resolution, absolute-dated Holocene and deglacial Asian monsoon record from Dongge Cave, China

Carolyn A. Dykoski[a,*], R. Lawrence Edwards[a], Hai Cheng[a], Daoxian Yuan[b], Yanjun Cai[c], Meiliang Zhang[b], Yushi Lin[b], Jiaming Qing[b], Zhisheng An[c], Justin Revenaugh[a]

[a]*Department of Geology and Geophysics, University of Minnesota, MN 55455, USA*
[b]*Karst Dynamic Laboratory, The Ministry of Land Resources, 40 Qixing road, Guilin 541004, China*
[c]*State Key Lab of Loess and Quaternary Geology, Institute of Earth Environment, Chinese Academy of Sciences, Xi'an, 710075, China*

Received 24 May 2004; received in revised form 20 January 2005; accepted 25 January 2005
Available online 23 March 2005
Editor: E. Boyle

Abstract

We present a continuous record of the Asian monsoon over the last 16 ka from $\delta^{18}O$ measurements of stalagmite calcite. Over 900 oxygen isotopic measurements providing information on shifts in monsoon precipitation are combined with a chronology from 45 precise ^{230}Th dates. $\delta^{18}O$ and therefore Asian monsoon intensity generally follows changes in insolation, although changes in $\delta^{18}O$ are generally accommodated in abrupt shifts in contrast to smoothly varying insolation, indicating that threshold effects may be important. $\delta^{18}O$ decreased dramatically (~3‰) at the start of the Holocene (~11.5 ka) and remained low for ~6 ka. Four positive $\delta^{18}O$ events centered at 11225±97 yr BP (1.05‰), 10880±117 yr BP (1.15‰), 9165±75 yr BP (1.4‰), and a double event centered at 8260±64 yr BP (1.1‰) and 8080±74 yr BP (1.0‰) punctuated this period of high monsoon intensity. All four events correlate within error with climate changes in Greenland ice cores. Thus, the relationship between the Asian monsoon and the North Atlantic observed during the glacial period appears to continue into the early Holocene. In addition, three of the four events correlate within error with outburst events from Lake Agassiz. The decline of monsoon intensity in the mid-late Holocene is characterized by an abrupt positive shift in $\delta^{18}O$ which occurs at 3550±59 yr BP (1.1‰ in ~100 yr). In addition, the Holocene is punctuated by numerous centennial- and multi-decadal-scale events (amplitudes 0.5 to 1‰) up to half the amplitude of the glacial interstadial events seen in the last glacial period. Thus, Holocene centennial- and multi-decadal-scale monsoon variability is significant, although not as large as glacial millennial-scale variability. The monsoon shows a strong connection with northern South American hydrological changes related by changes in ITCZ position. Spectral analysis of the $\delta^{18}O$ record shows significant peaks at solar periodicities of 208 yr and 86 yr suggesting variation is influenced by solar forcing. However, there are numerous other significant peaks including peaks at El Niño frequencies (observed for high-resolution portions of the record between 8110 and 8250 yr) which suggest that changes in oceanic and atmospheric circulation patterns in addition to those forced by solar changes are important in controlling Holocene monsoon

* Corresponding author. Tel.: +1 612 624 9598; fax: +1 612 625 3819.
E-mail address: dyko0008@umn.edu (C.A. Dykoski).

0012-821X/$ - see front matter
doi:10.1016/j.epsl.2005.01.036

climate. In addition, for this high-resolution portion, we observe a distinctive biennial oscillation of the Asian monsoon, which has been associated with the Tropospheric Biennial Oscillation (TBO).

Keywords: speleothem; Asian monsoon; Holocene; inductively coupled plasma; China

1. Introduction

The stability (or instability) of interglacial climate has become an important issue that can be addressed by studying Holocene climate. Recently, a millennial-scale pattern, which occurs during the last glacial period [1], has been observed to extend into the Holocene [2,3], challenging the idea of fairly stable climatic conditions observed in Greenland ice cores during the Holocene. If climate is driven by solar forcing, the tropics would be a likely candidate for picking up the signal and then amplifying it to the rest of the world due to the large amount of radiation that the Earth receives at those latitudes and the physics of heat transport [4]. Some of the cycles observed in the solar spectra have decadal-scale variation and would require a high-resolution proxy to record the potential signal. The Greenland and Antarctic ice cores are complete, high-resolution records of the Holocene and are fairly well-dated, but are restricted to polar regions.

High-resolution, precisely dated records from the lower latitudes, which cover a good portion of the Holocene, are useful in resolving these issues [5–7]. Speleothems can have continuous deposition of calcium carbonate over long periods of time and well-chosen speleothems are datable with high precision. Absolute ages can be determined by means of ^{230}Th dating by mass spectrometry [7]. Here, we present a high-resolution Holocene record based upon a speleothem recovered from Dongge Cave in south China.

Previous work on speleothems recovered from Hulu Cave, near Nanjing, China, shows large and at times rapid shifts in monsoon intensity between 75 ka and 11 ka [8]. The speleothems from Hulu Cave were deposited near the eastern coast of China at a locality affected only by the East Asian monsoon. The long-term trend in δ^{18}O correlates to summer insolation values at that latitude (33°N), suggesting summer monsoon enhancement through increases in the temperature differences between the continent and ocean. Similarities between the oxygen isotope record from the Greenland ice core and the Chinese record are strong [8]. Features similar to Dansgaard/Oeschger [9] events are observed in the Chinese record, demonstrating a strong link between the East Asian monsoon and North Atlantic climate for the last glacial period and deglacial sequence. This evidence suggests that circulation changes hypothesized to cause the Dansgaard/Oeschger events [10] may have also affected the tropical western Pacific Ocean where the East Asian monsoon originates.

Dongge Cave is different from the Hulu Cave samples in two ways. It is located inland from the coast to the south and west relative to Hulu Cave. Secondly, the Dongge cave speleothem that is the main focus of this work spans Holocene as well as (late Pleistocene) deglacial climate as opposed to the Hulu Cave speleothems which at present are largely restricted to the Pleistocene. Therefore, the Dongge Cave record can be used to test the extent to which the link between Asian monsoon intensity and Greenland climate continues into the Holocene. In addition, recent studies suggest that Dongge Cave is located in a region of China affected by the Indian monsoon [11]. Therefore, correlation with the Hulu Cave stalagmites during periods of concurrent growth would test whether or not mechanisms affecting the East Asian monsoon actually affect a broader region of the Asian monsoon system.

2. Location, local meteorology, and sample description

Stalagmite D4 was recovered from Dongge Cave, China (25°17′N, 108°5′E, elevation=680 m). The cave is located 18 km southeast of Libo, Guizhou Province in southern inland China (Fig. 1). Work from Dongge Cave was previously reported for stalagmites D3 and D4 as well as current climate conditions near

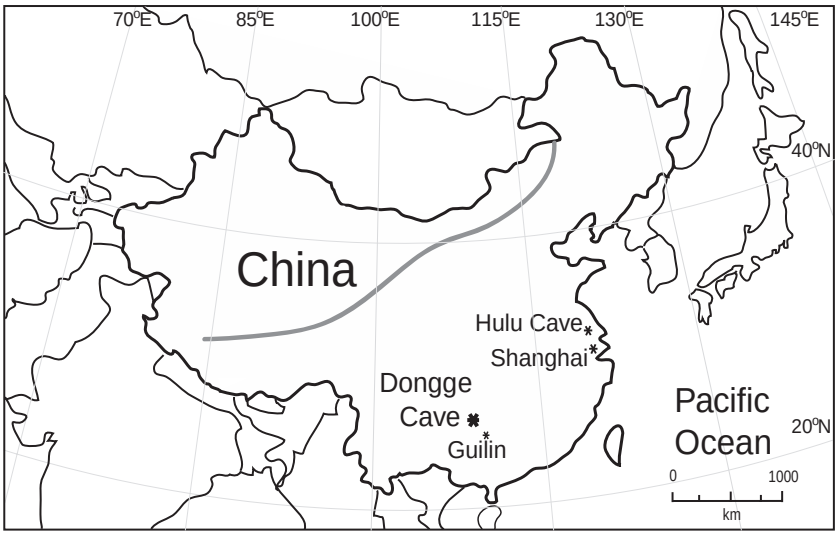

Fig. 1. A map of China showing the location of Dongge Cave (108°5′E, 25°17′N). It is located 1200 km southwest of Hulu Cave. The thick gray line designates the northernmost extent of the Asian summer monsoon.

Dongge Cave and the surrounding area (see Table S1 in the Appendix) [12]. Current air temperature in the cave is 15.6 °C. Mean annual meteoric precipitation near Dongge Cave is 1753 mm with monthly values given in Table S1 in the Appendix. This area is strongly affected climatically by the Asian monsoon system. Most of the rainfall (80%) occurs during the summer monsoon months (May–Oct), with much less precipitation (20%) occurring during the winter monsoon months (Nov–Apr). Oxygen isotope ratios [reported relative to Vienna Standard Mean Ocean Water (VSMOW)] from rainwater collected in Guiyang (26°35′N, 106°43′E; elevation=1071 m, 160 km NW of Dongge Cave) range between −3.4‰ in the winter and −12.4‰ in the summer with an annual average of −8.3‰.

D4 was collected 500 m from the cave entry and ~100 m below the surface. Its total length is 304 cm and its diameter ranges between 12 and 20 cm (see Fig. S1 in the Appendix). At the time of collection, water was actively dripping suggesting deposition occurred until the present. Growth of D4 occurred in three intervals: 148 to 113 ka, 65 to 43 ka and 16 ka to present. Yuan et al. [12] and Kelly et al. [13] examine in detail the two older periods of growth, which includes the last interglacial period and portions of both the most recent and penultimate glacial periods, while the most recent growth is discussed in this study. Although some Holocene data were reported by Yuan et al. [12], we report here much higher resolution oxygen isotope data and dating.

3. Analytical methods

3.1. Stable isotopes

First, the sample was halved along the growth axis and the surface polished. Each sample was milled using carbide dental burrs ranging in size from 0.3 to 0.9 mm along the length of the speleothem parallel to the central growth axis. Preparation steps are similar to those described in Dorale et al. [14]. Spacing between samples ranged from 1 cm to 0.5 mm, with typical powder masses of 80 to 100 μg.

Stable isotope ratios of oxygen ($^{18}O/^{16}O$) and carbon ($^{13}C/^{12}C$) were measured for 907 samples. The analyses were performed in two locations: (1) Institute of Earth Environment, Xi'an, China and (2) the Minnesota Isotope Laboratory, Minneapolis, USA. Both locations use a Finnigan-MAT 252 mass spectrometer fitted with a Kiel Carbonate Device III. Standards were run every 10 to 15 samples and duplicates were run every 10 to 20 samples to check for homogeneity. NBS18 and NBS19 were run in both locations and the error was 0.04 to 0.10‰. Duplicates

replicated within 0.16‰ for oxygen (most below 0.10‰) and 0.20 ‰ for carbon (with the exception of two sample pairs which were most likely due to sampling error). The Chinese lab used a highly purified CO_2 gas ($\delta^{18}O$=21.28‰, $\delta^{13}C$=24.74‰) as a reference for standardizing samples. At Minnesota, the Laboratory Information Management System (LIMS) was used to normalize the raw data to VPDB (‰), instead of standardizing the reference gas. To test for systematic offsets between the results from the two laboratories, we examined the few short portions of the record with alternating analyses from each laboratory. We analyzed groups of three consecutive analyses and compared the middle with the average of the other two. For 90 such calculations, the average difference between the two values was 0.00‰ with a standard deviation of 0.22. As this difference is due to both climate and analytical offset we infer that analytical offset is negligible. Values are reported as $\delta^{18}O$ (‰) and $\delta^{13}C$ (‰) with respect to the Vienna Pee Dee Belemnite (VPDB) standard.

3.2. ^{230}Th dating

Samples for dating were drilled using carbide dental burrs following stratigraphic horizons as in Dorale et al. [14]. Typical powder amounts ranged from 100 to 300 mg. The chemical procedure used to separate the uranium and thorium is similar to that described in Edwards et al. [7]. The calcite powder is dissolved with nitric acid, a mixed $^{229}Th/^{233}U/^{236}U$ tracer is added, and the sample is dried down. After the addition of an iron chloride solution, NH_4OH is added drop by drop until the iron precipitates. The sample is then centrifuged to separate the iron from the rest of the solution and the overlying liquid is removed. After loading the sample into columns containing anion resin, HCl is added to elute the thorium and water is added to elute the uranium. With the uranium and thorium separated, each sample is dried down and dilute nitric acid is added for injection into the ICP-MS.

Analyses were conducted by means of inductively coupled plasma mass spectrometry (ICP-MS) on a Finnigan-MAT Element outfitted with a double focusing sector-field magnet in reversed Nier–Johnson geometry and a single MasCom multiplier. The instrument was operated at low resolution and in electrostatic peak hopping mode. Combined ionization plus transmission efficiency of 2.5 to 3‰ has been measured for uranium and 1.5 to 2‰ has been measured for thorium. Further details on instrumental procedures are explained by Shen et al. [15].

4. Results

4.1. Replication

It is critical to have an accurate understanding of what the stable isotope results represent. Many processes other than climate may be involved in producing the $\delta^{18}O$ signal observed in speleothems. Kinetic fractionation, mixing of water during residence in the vadose zone, dissolution–reprecipitation, and degassing history can contribute to the $\delta^{18}O$ signal, therefore shifting the climate signal. A simple test is a replication test of isotopic records of stalagmites from the same cave [16]. Oxygen isotope results from another stalagmite retrieved from Dongge cave (D3) essentially replicate the oxygen isotopic record of D4 at periods when the two stalagmites grew contemporaneously (115 to 148 ka) [12]. The two samples grew 200 m apart and it is highly unlikely that the combination of conditions experienced by each set of drips was identical in each case. Therefore, kinetic fractionation and water–rock interactions are not likely to have had a large effect on D4 $\delta^{18}O$.

Furthermore, the deglacial portion of D4 precisely replicates the oxygen isotope record of the Hulu cave stalagmites (Fig. 2) [8]. It is important to note that this replication is not required as climate history in the two localities separated by 1200 km (Fig. 1) could well have been different. Slight differences occur, which are small compared to the amplitude of the record, and may not be significant in terms of climate. The fact that the records from the two localities replicate indicates that the $\delta^{18}O$ signal from both Dongge Cave and Hulu Cave is recording climatic changes and that changes in the monsoon are similar over a large area of China.

Another check is to test for correlation between $\delta^{18}O$ and $\delta^{13}C$ [17]. R^2 values are low (0.15; Fig. 3) suggesting kinetic fractionation has little effect and that the $\delta^{18}O$ signal is primarily of climatic origin. Therefore, we interpret $\delta^{18}O$ values in terms of

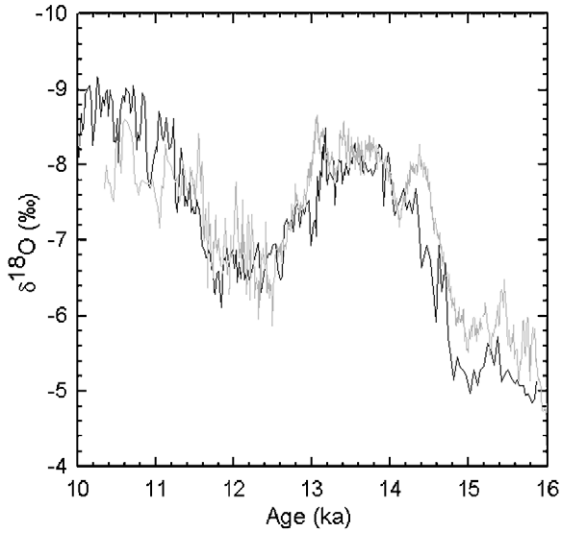

Fig. 2. The deglacial sequence of Dongge stalagmite D4 (black) and Hulu stalagmite H82 (gray) from 10 ka to 16 ka. Though, 1200 km apart, both D4 and H82 show a remarkably similar $\delta^{18}O$ pattern suggesting regional climatic variations are detectable in these two stalagmites.

temperature and $\delta^{18}O$ of meteoric precipitation. The high amplitude nature of the record from D4 (glacial/interglacial transition ~4‰) combined with the small water–calcite temperature-dependent fractionation (−0.23‰/°C) [18] leaves $\delta^{18}O$ of precipitation as the primary contributor to the $\delta^{18}O$ signal recorded in the speleothem.

Changes in $\delta^{18}O$ of precipitation can result from changes in $\delta^{18}O$ of the sea water source as well as air mass transit variability between the source waters and the cave site. Changes in the isotopic composition of source waters are possible through a change in salinity, which involves two main factors: (1) local hydrology of the source regions and (2) deglaciation. The full history of salinity changes in plausible sea water sources for the monsoon is unknown. However, one data set from the South China Sea shows a small difference in $\delta^{18}O$ between the mid-Holocene and modern conditions of 0.15‰ [19].

Deglaciation would cause an average decrease in ocean salinity such that $\delta^{18}O$ would change by ~1‰ [20]. If shifts in sea level are always proportional to $\delta^{18}O$ changes during deglaciation, we can use the deglacial sea-level curve [21,22] to calculate decreases in $\delta^{18}O$ of ~0.15‰ prior to 16 ka, an additional decrease of ~0.35‰ between 16 and 11.5 ka, and a final decrease of ~0.5‰ during the first half of the Holocene [23]. This effect is relatively small compared to the shift of 4‰ in the record. Therefore, we have not corrected for this effect and most of the difference in $\delta^{18}O$ in Dongge Cave must be due to changes in $\delta^{18}O$ during air mass transit.

We have previously discussed two explanations for changes in the $\delta^{18}O$ of monsoon precipitation. Wang et al. [8] used changing ratios of summer to winter precipitation to interpret the high amplitude changes in $\delta^{18}O$. This explanation relies on the fact that summer monsoon rains dominate the annual precipitation budget and are distinctly lighter isotopically than winter precipitation.

Yuan et al. [12] observed that other northern low-latitude sites around the world (Venezuela, [24]; and Israel, [25]) record $\delta^{18}O$ changes similar to China that are inverted with respect to the $\delta^{18}O$ record in Greenland. However, these sites do not record the strong seasonal difference in precipitation observed in China. To broaden the interpretation of $\delta^{18}O$ values to these other sites, Yuan et al. [12] modified the previous explanation by describing how changes in the percentage of water vapor lost prior to reaching the subtropics varied over time using a Rayleigh fractionation model [26]. Integrated rainfall from

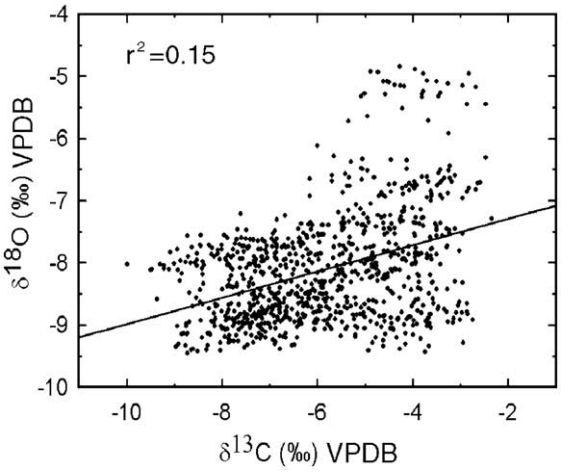

Fig. 3. $\delta^{13}C$ versus $\delta^{18}O$ from stalagmite D4. Simultaneous shifts in $\delta^{13}C$ and $\delta^{18}O$ would demonstrate a linear correlation and indicate kinetic effects dominate the isotopic signal. The low correlation (r^2=0.15) of the plotted results indicates that carbon and oxygen are not highly correlated through kinetic fractionation.

tropical sources to SE China during glacial times was calculated to be 65% of that during the mid-Holocene [12]. Thus, following this interpretation, changes in the proportion of precipitation reaching China correlate with changes in Greenland temperature. The Yuan et al. [12] mechanism provides a single explanation for the fact that the $\delta^{18}O$ relationship seen in the northern tropics and subtropics at multiple sites is inverted with respect to Greenland.

4.2. Chronology

Previous work has shown that deposition of D4 occurred during 3 periods of growth at 148 to 113 ka, 66 to 42.5 ka, and 16 ka to present, which were interrupted by 2 hiatuses [12]. Most of the growth (~2.0 m out of 3.04 m) occurred since the last hiatus (since 16 ka: the last deglacial sequence and Holocene). 45 ^{230}Th dates were acquired within the youngest growth phase. Decay constants and measured values of uranium and thorium concentrations used in these calculations are listed in Table 1. Concentrations range between 170 to 500 ppb for ^{238}U and 0.01 to 0.9 fg of ^{230}Th/g of sample. Ages were corrected using an initial $^{230}Th/^{232}Th$ atomic ratio of $(7.0\pm5.0)\times10^{-6}$. This value was calculated using samples with anomalously high concentrations of ^{232}Th together with the constraint of stratigraphic order. For almost all the samples, the correction for initial ^{230}Th was negligible. Dates are reported with 2σ analytical errors that average $\pm$67 yr (and range between 19 and 138 yr).

All of our dates occur in stratigraphic order and it appears that D4 grew continuously throughout this period. Linear interpolation was used to calculate an age for each $\delta^{18}O$ value. To determine the error for a linearly interpolated age, the normal procedure would involve combining appropriately weighted errors from the measured ICP-MS ages on either side of the sample quadratically. This procedure would generally produce an error in interpolated age, which is less than the error in age of the actual measured bounding ages. Such an error estimate is not likely valid as no term for error in changes in growth rate has been applied, nor is it possible to quantify such a term. Thus, the true error is most likely greater than that calculated with the quadratic method. We arbitrarily chose to calculate the error by adding the appropriately weighted bounding age errors linearly, providing a more reasonable error estimate. In one case (9105$\pm$416 yr BP), the error was very large due to a high ^{232}Th concentration correction. This age was omitted during the above error calculations.

Growth rate varied within the sample from ~20 to 500 μm/yr with an average of 154 μm/yr during the Holocene, 43 μm/yr during the deglacial sequence and 122 μm/yr for the whole record (Figs. 4 and 5). Between 7.5 and 8.5 ka, growth rate reached as high as 500 μm/yr. This period of high growth rate corresponds to the period of lightest $\delta^{18}O$, which we infer to be the time of highest rainfall (see below). Overall, the changes in growth rate are broadly consistent with changes in precipitation inferred from $\delta^{18}O$ data. High growth rates are ideal for high-resolution sampling of oxygen isotope ratios, as we can achieve a sampling resolution of about 300 μm even drilling by hand.

4.3. The $\delta^{18}O$ record

The sampling interval of D4 yielded an average time resolution of ~19 years with some portions sampled as high as every 1 to 2 yr. The presence of annual bands was not observed. The D4 profile of $\delta^{18}O$ shows many distinct features (Fig. 6). Note that $\delta^{18}O$ is plotted increasing downwards. At the start of growth ~16 ka, $\delta^{18}O$ values are relatively heavy (−5‰) and growth rate is relatively low. Bands within the sample are well defined and dark gray in color. A dramatic shift toward lighter values (~3‰) occurs at 14.7 ka, coincident within error with the start of the Bolling–Allerod in Greenland. These light values (−8‰) were maintained for ~1.7 ka. At ~13 ka, $\delta^{18}O$ begins to rise and by 12.5 ka had risen by 2‰ to heavier values. This event corresponds to the beginning of the Younger Dryas as recorded in Greenland. At ~11.5 ka, $\delta^{18}O$ falls to lighter values of −8.4‰, within error of the end of the Younger Dryas. After this abrupt drop, $\delta^{18}O$ values continue to get lighter gradually until they reach peak values between 8 and 9 ka.

This general decrease in $\delta^{18}O$ is interrupted by 11 heavy excursions between 11.5 and 8 ka. The four largest (amplitudes greater than 1.0‰) occur at 11.2, 10.9, 9.2, and 8.1/8.2 ka and last between 90 and 230 yr. The first event occurs within error of the Preboreal

Table 1
^{230}Th dating results from stalagmite D4 from Dongge Cave, China

Sample number	Depth (mm)	^{238}U (ppb)	^{232}Th (ppt)	^{234}U* (measured)	^{230}Th/^{238}U (activity)	^{230}Th age (years, BP) (uncorrected)	^{230}Th age (years, BP) (corrected)	$^{234}U_{Initial**}$ (corrected)
B1-1	4	430±0.75	1.6±47	−1.1±1.9	0.00134±0.0002	93±22	**93±22**	−1.1±1.9
B1-2	30	440±1.25	93.8±22	−5.2±3.3	0.00224±0.00017	246±19	**183±21**	−5.2±3.3
B2-5	82	495±0.94	122±24	−2.3±1.8	0.00415±0.00017	403±19	**391±20**	−2.3±1.8
B2-2	125	409±0.57	272±23	−11.7±1.5	0.00899±0.00022	945±24	**914±33**	−11.8±1.5
B2-4	135	276±0.85	240±21	−8.9±4.8	0.00991±0.00026	1044±29	**1003±41**	−8.9±4.8
B2-3	205	360±0.52	53.8±23	−14.4±1.5	0.01215±0.00028	1301±32	**1294±32**	−14.4±1.5
B2-1	227	212±0.36	0±47	−7.2±2.4	0.01349±0.00062	1441±69	**1442±70**	−7.3±2.4
B3-9	264	352±0.64	117±23	−10.7±1.7	0.01934±0.00040	2103±46	**2088±47**	−10.8±1.7
B3-3	286	252±0.32	172±23	−19.9±1.5	0.0231±0.00047	2551±22	**2519±59**	−20.0±1.5
B3-11	307	352±0.45	297±15	−8.8±1.4	0.02437±0.00119	2666±135	**2627±138**	−8.9±1.4
B3-6	330	173±0.22	55.3±23	−16.2±1.7	0.02916±0.00047	3233±55	**3218±56**	−16.3±1.7
B3-13	339	200±039	57±21	−11.4±12.2	0.03285±0.00051	3637±59	**3625±60**	−11.4±2.2
B3-10	396	472±0.59	1060±24	−2.5±1.2	0.03756±0.00033	4138±38	**4034±84**	−2.5±1.2
B3-7	465	301±0.49	207±23	−2.0±1.6	0.03798±0.00040	4184±46	**4152±51**	−2.1±1.6
B3-5	488	452±0.53	60.5±23	−6.0±1.3	0.03855±0.00043	4267±50	**4260±50**	−6.0±1.3
B3-4	545	165±0.22	40.0±23	−14.0±1.8	0.04148±0.00074	4641±86	**4629±87**	−14.2±1.8
B3-12	598	269±0.30	21.8±15	0.8±1.2	0.04675±0.00049	5171±56	**5167±57**	0.8±1.3
B3-1	640	386±0.68	29±45	−10.9±2.1	0.04806±0.00093	5387±109	**5383±109**	−11.1±2.2
B4-2	789	324±0.43	116±23	−24.6±1.3	0.05078±0.00043	5786±51	**5769±53**	−25.0±1.3
B4-5*	916	329±0.73	307±15	−9.3±1.9	0.05656±0.00042	6367±51	**6324±60**	−9.5±2.0
B4-1	985	270±0.35	130±24	−2.9±1.5	0.05869±0.00053	6571±62	**6549±64**	−2.9±1.6
B4-4	1092	474±0.57	64±15	1.1±1.2	0.06265±0.00031	7004±38	**6998±38**	1.1±1.2
B5-1	1212	265±0.31	41.3±21	−8.1±1.3	0.06549±0.00051	7406±61	**7399±62**	−8.2±1.3
B5-2	1258	373±0.46	84±13	−16.3±1.3	0.06741±0.00035	7698±43	**7687±44**	−16.3±1.3
B6-3	1412	338±0.51	137±0.22	−28.3±1.6	0.06968±0.00059	8076±73	**8056±74**	−28.9±1.6
B6-4	1482	230±0.30	20.2±23.1	−8.7±1.6	0.07216±0.00062	8201±75	**8197±75**	−8.9±1.6
B6-9*	1548	385±0.97	196±15	−15.5±2.3	0.07413±0.00048	8496±61	**8472±64**	−15.8±2.3
B6-2	1626	289±0.40	101±22	−0.4±1.5	0.07873±0.00060	8906±72	**8890±73**	0.4±1.6
B6-1	1638	249±0.74	3019±23	−2.8±4.6	0.08494±0.00080	9669±107	**9105±416**	−2.9±4.7
B6-8	1653	309±0.36	439±14	−16.3±1.3	0.08328±0.00050	9609±62	**9542±78**	−16.3±14
B6-5	1668	294±0.54	219±24	−15.8±1.8	0.08664±0.00088	10012±109	**9977±112**	−16.2±1.9
B6-7	1691	314±0.39	458±15	−7.3±1.5	0.09116±0.00048	10465±60	**10,397±77**	−7.3±1.5
B7-8	1717	372±0.71	217±23	−7.1±1.9	0.09497±0.00093	10927±116	**10,890±118**	−7.3±1.9
B7-1	1742	366±0.45	354±23	−8.8±1.3	0.09879±0.00065	11414±82	**11,368±88**	−9.1±1.3
B7-9	1763	452±1.25	265±15	−18.7±2.5	0.10051±0.00086	11751±86	**11,723±88**	−19.4±2.5
B7-7	1783	428±0.82	117±23	−15.6±1.8	0.10415±0.00061	12162±80	**12,149±81**	−16.2±1.9
B7-2	1795	386±0.66	465±22	−27.7±1.6	0.10610±0.00062	12571±81	**12,514±91**	−28.7±3.3
B7-3	1812	348±0.59	73.1±23	−17.6±1.6	0.11069±0.00069	13005±90	**12,995±90**	−18.2±1.7
B7-6	1833	372±0.62	23.9±24	−4.9±1.6	0.11350±0.00074	13172±95	**13,169±95**	−5.0±1.6
B7-4	1844	287±0.49	72.3±22	1.4±1.7	0.11427±0.00077	13170±97	**13,165±98**	1.5±1.7
B7-5	1869	302±0.88	98.4±23	−9.4±3.0	0.11682±0.00074	13653±103	**13,638±104**	−9.8±3.2
B8-2	1886	284±0.52	78.1±22	−8.3±1.7	0.12077±0.00079	14130±103	**14,117±103**	−8.6±1.8
B8-3	1905	259±0.46	397±23	−5.4±1.8	0.12732±0.00078	14907±102	**14,835±114**	−5.6±1.9
B8-4	1921	327±0.52	81.4±23	0.0±1.5	0.13317±0.00072	15552±94	**15,541±95**	0.0±1.5
B8-1	1935	406±0.55	562±22	−11±1.4	0.13511±0.00074	15983±97	**15,918±108**	−11.0±1.4

The error is 2σ error. Decay constant values are $\lambda_{230}=9.1577\times10^{-6}$ yr^{-1}, $\lambda_{234}=2.8263\times10^{-6}$ yr^{-1}, $\lambda_{238}=1.55125\times10^{-10}$ yr^{-1}. Corrected ^{230}Th ages assume an initial ^{230}Th/^{232}Th atomic ratio of $(7.0\pm5.0)\times10^{-6}$. Samples B4-5 and B6-9 are marked with an * to designate the replacement of samples B4-3 and B6-6 (respectively). B4-3 and B6-6 had ages out of stratigraphic order that are most likely due to a handling error. Samples B4-5 and B6-9 were redrilled along the same growth horizons as the previous samples and gave ages within stratigraphic order. ^{230}Th ages are indicated in bold.

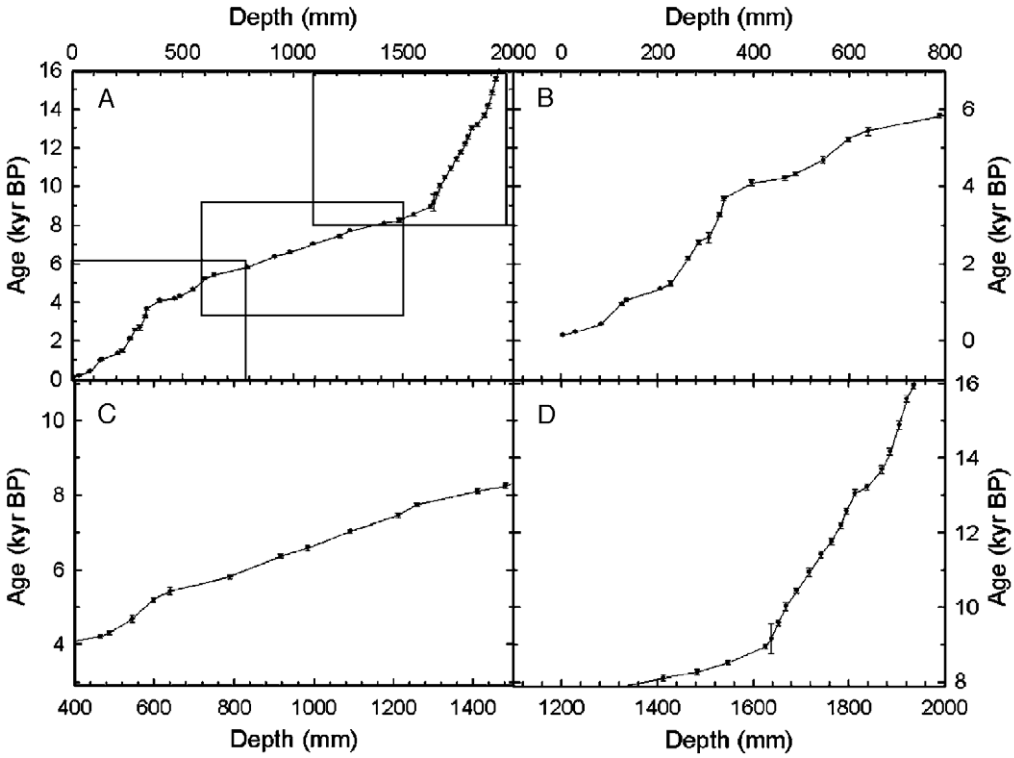

Fig. 4. Plot of age versus depth for stalagmite D4. (A) Full record, (B) 0 to 7 ka, (C) 3 to 11 ka, (D) 8 to 16 ka. Growth is continuous from 16 ka to present, though the growth rate changes periodically. Error bars indicate 2σ error.

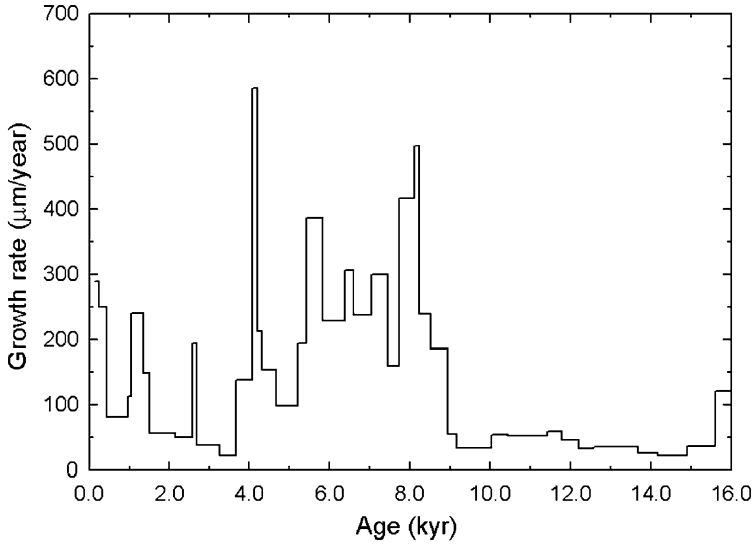

Fig. 5. Growth rate versus time for stalagmite D4. Growth rate is fairly constant until 9 ka, where the rate increases and becomes more variable. Highest rates of growth occur ~8 to 9 ka.

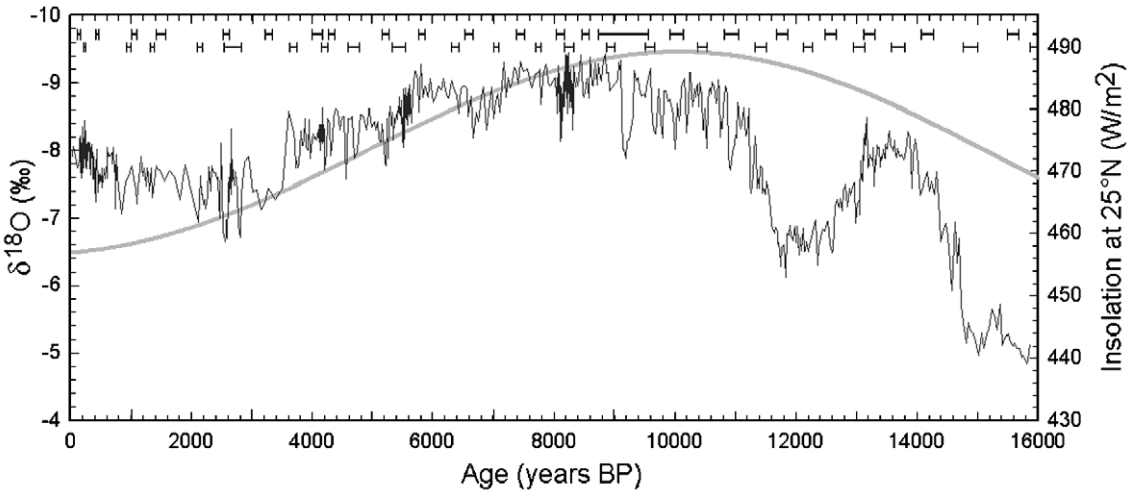

Fig. 6. Stalagmite D4 oxygen isotope values versus time (black) and average summer insolation for 25°N (gray). 45 ^{230}Th ages are also plotted with 2σ error bars.

Oscillation (11.2 ka, 1.05‰) observed in the ice cores from Greenland. The second event occurs at 10.9 ka (1.15‰) and also correlates with a climate shift in Greenland. The largest of the early Holocene events occurs at 9.2 ka, when δ^{18}O shifts to heavier values by 1.4‰. This is similar to an event observed in the NGRIP ice core at 9.2 ka. The last of the heavy δ^{18}O excursions in the early Holocene exists as two shifts in δ^{18}O (~1‰), which occur at 8260 and 8080 yr BP and correlates within error with the 8200 yr BP Event observed in Greenland. Growth rate, which had remained relatively constant at values of ~40 μm/yr until this point, increases at ~9 ka by over a factor of 10 and remains high for ~1000 yr (Fig. 5). After this period of high growth rate, growth rate decreases but remains ~100 to 400 μm/yr throughout the middle Holocene. At ~6.8 ka, δ^{18}O values begin to lighten until a low of −9‰ is reached ~6 ka. At this point, δ^{18}O values again reverse toward heavier values with an increase of 1.5‰ in 570 yr and growth rate slows to ~100 μm/yr. From ~5.2 ka to 3.5 ka, δ^{18}O does not show an increasing or decreasing trend, but appears to fluctuate around a value of −8.2‰. At ~4 ka, growth slows to near minimum values of 20 μm/yr. Following the period of steady δ^{18}O, an abrupt positive shift occurs at 3550±59 yr BP (1.15‰ in 100 yr). This is followed by a period of high amplitude changes in δ^{18}O (up to 1.6‰) which occurs for ~1.5 ka. Over the last 2 ka, there is a slight decrease towards lighter δ^{18}O values until modern values of about −8‰ are reached.

Throughout the Holocene, δ^{18}O varies continually. Several significant events occur in the early Holocene including an event at 11.2 ka BP and 10.9 ka BP, the prominent feature at ~9.3 ka BP and the double event ~8.2–8.1ka BP. High frequency variability of ~0.5 to 1‰ persists during the middle–late Holocene. The largest δ^{18}O change in the middle to late Holocene is observed at ~3.5 ka with a sharp unidirectional event. Growth rate broadly follows trends in δ^{18}O as increases in growth correlate with periods of light δ^{18}O. This relationship supports the idea that changes in integrated precipitation are the ultimate cause of changes in the δ^{18}O record [12].

4.4. Spectral analysis

Spectral analysis was performed on the δ^{18}O record from Dongge Cave using the program MTAP [27]. The multi-taper method approach used a bandwidth factor of 3 and 5 tapers (degrees of freedom) at high resolution. Fig. 7 shows four different time series that were analyzed. First, the whole data set (~16 ka to present, including both the deglacial and Holocene portions of the record) was run with an average sampling of 19 yr per sample, thereby giving a cutoff interval of reliable periodicities at ~40 yr. These results are given in Fig. 7A and

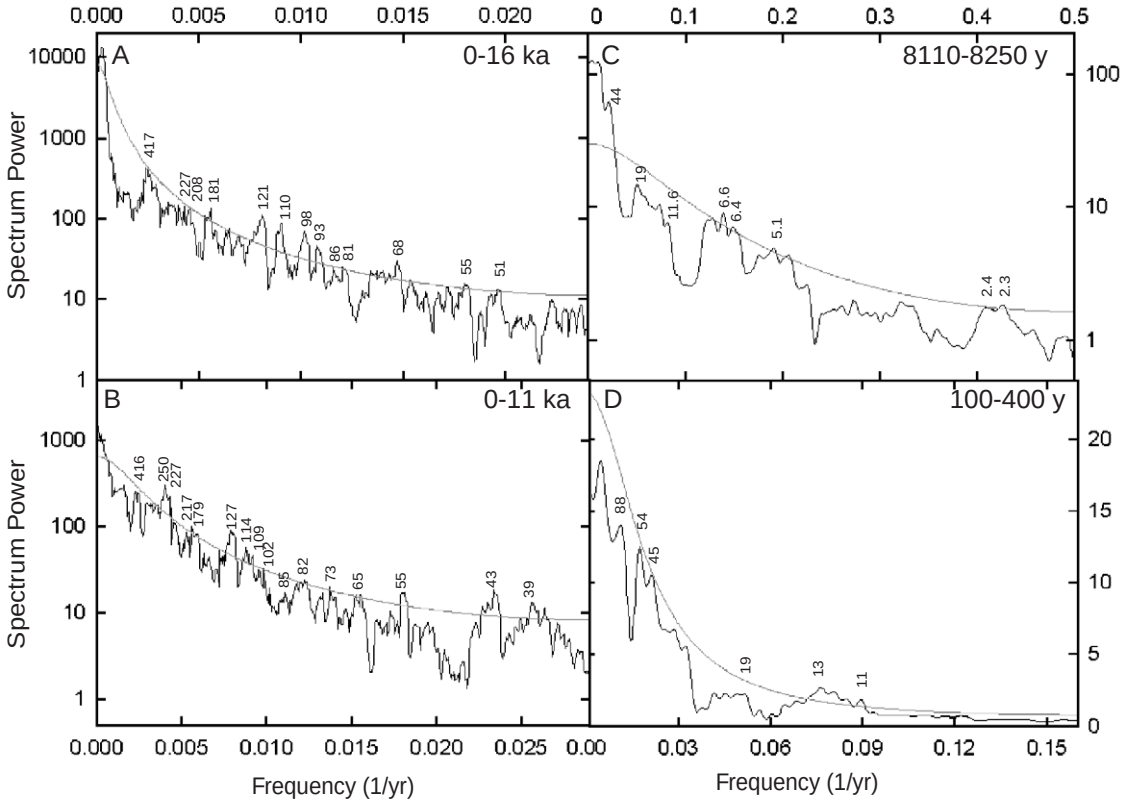

Fig. 7. Spectral analysis results for D4. (A) Full $\delta^{18}O$ record (~16 ka to present), (B) Holocene (~11 ka to present), (C) high resolution $\delta^{18}O$ record from 8110 to 8250 yr, and (D) high resolution $\delta^{18}O$ record from 100–400 yr. Peaks are labeled with their period in years. Due to different sampling intervals, the Nyquist frequency or reliable cutoff frequency varies for each run. Each plot shows only those frequencies that are below the Nyquist frequency. Note the different scales for each plot.

show statistically significant periodicities at the 90% confidence level at 417, 227, 208, 181, 121, 110, 98, 93, 86, 81, 68, 55, and 51 yr. A second portion of the record that contained only the Holocene (~11 ka to present) was examined which has a slightly higher sampling interval of 15 yr per sample. These results are shown in Fig. 7B and are very similar to Fig. 7A. Two high-resolution portions of the record were also examined (Fig. 7C and D). The first consisted of 140 yr of the data from 8110 to 8250 yr BP with an average sampling of ~1 yr per sample, thereby giving a cutoff interval of ~2 yr. These results are given in Fig. 7C and show significant periodicities at 44, 6.6, 6.4, 5.1, 4.8, 2.4–2.3 yr. Fig. 7D shows the results of the other high-resolution portion of the data from 100 to 400 yr BP. This time interval is double the length of the previous run but has lower resolution sampling averaging at 3 yr per sample. This makes it impossible to determine periodicities less than 6 yr. Fig. 7D shows the addition of peaks at 13 yr and 11 yr periodicities.

5. Climate discussion

Stalagmite D4 shows features similar to deglacial features seen in Greenland, including the Bolling/Allerod and Younger Dryas periods. This correlation agrees with the results from Hulu Cave [8], thus confirming that the relationship between the monsoon and Greenland temperature is maintained throughout the deglacial sequence as well as broadening the relationship between the Asian monsoon and North Atlantic climate to a larger area of China [12].

The four early Holocene events that correlate within dating error with events from Greenland (Fig. 8) are as follows. The first event, noted as the Preboreal Oscillation in the North Atlantic [28], is centered at 11360±227 yr BP in GISP2 [29,30] and 11340±30 yr BP for NGRIP [31]. D4 shows an event at 11225±97 yr BP. The second event is centered at 10850±217 yr BP in GISP2 and 10850±30 yr BP in NGRIP, while D4 shows an event at 10880±117 yr BP. The third event is recorded in NGRIP (9260±30 yr BP) and closely resembles the event recorded in D4 at 9165±75 yr BP. Two possibilities exist for an event in D4 that correlates with the "8.2 ka Event" in Greenland. The first is centered at 8260±64 yr BP and the second is centered at 8080±74 yr BP. The 8.2 ka Event as recorded in the GISP2 core is centered at 8210±160 yr BP and in the NGRIP core the event is centered at 8200±30 yr BP [31]. Though the three records exhibit some variability in the timing, it is possible that either of the events seen in China ~8.1/8.2 ka correlates with the event seen in Greenland.

A number of the events observed in Greenland in the early Holocene have been linked to outburst events from Lake Agassiz [32,33]. It is possible these large influxes of water could have altered North Atlantic salinity in such a way to affect ocean circulation triggering widespread deglacial climate oscillations [34,35]. Of our four large heavy excursions, three correlate with outburst events. Many of the smaller events in the early Holocene could

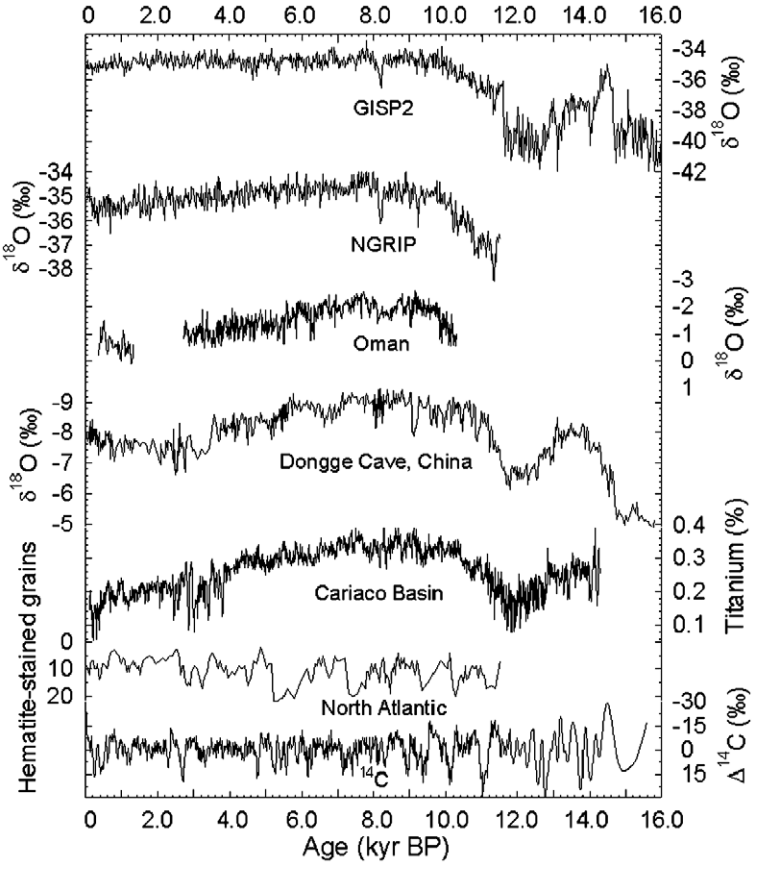

Fig. 8. A comparison of the D4 record from Dongge Cave, China to several Holocene records from 16 ka to present. (A) GISP2 δ^{18}O record from Greenland [30], (B) NGRIP δ^{18}O record from Greenland [31], (C) Indian monsoon variation represented by δ^{18}O in stalagmite Q5 from Oman [6], (D) δ^{18}O record of the Asian monsoon from Dongge cave, China, (E) titanium (%) data from the Cariaco Basin [44], (F) percentage of hematite-stained grains in core VM29-191 from the North Atlantic [2], and (G) detrended decadal atmospheric Δ^{14}C [50].

correlate with outburst events but dating uncertainties preclude making a precise correlation. The Greenland/Dongge Cave correlations indicate that the close relationship observed during the glacial period between the monsoon and Greenland climate [8] extends into the early Holocene. However, subsequent to 8 ka, stalagmite D4 shows proportionally more $\delta^{18}O$ variability than GISP2 and NGRIP.

The trend toward increasingly lighter $\delta^{18}O$ values in the early Holocene and then decline toward heavier $\delta^{18}O$ values in the mid–late Holocene follows the general trend of incoming solar radiation (Fig. 6). Correlation between monsoon intensity and insolation has been predicted [36] and demonstrated [8,37–39] by other records of the monsoon. However in the Holocene, peak monsoon intensity and peak insolation values do not exactly coincide as they do in the last interglacial and glacial periods. As observed in other Holocene monsoon records [6,40], maximum monsoon intensity appears to lag insolation by 2 to 3 ky. To explain this observation, a correlation between monsoon strength and North Atlantic warmth in the early–mid Holocene [40] suggests that glacial climate boundary conditions, in addition to solar insolation, influenced climate at this time. It was only after the ice sheets had retreated that insolation began to dominate the monsoon. The D4 monsoon record provides evidence to support this as a possible explanation.

Into the mid–late Holocene as solar radiation values decline, the strength of the summer monsoon decreases. Previous records of Asian monsoon intensity show a gradually weakening monsoon that appears to mimic the smooth, declining radiation values [40,41]. The Dongge Cave stalagmite, D4, does not show this gradual decline. In fact, it shows a series of sharp drops in monsoon intensity throughout the Holocene. The interval between 5650 and 5220 yr BP is characterized by a generally weakening monsoon. An initial small, but abrupt drop occurs at 5650±70 yr BP followed by a trend toward heavy $\delta^{18}O$ values lasting ~400 yr. This interval coincides with the abrupt decrease of moisture in the African continent and the end of the African humid period (~5490±190 yr BP) [42]. A study using paired *t*-tests of multiple proxies of the Asian monsoon from eastern Africa to northeast China also found evidence for a sharp drop in monsoon intensity ~4.5 to 5 ka [43]. In our record, a second, larger decrease in monsoon intensity occurred at 3550±59 yr BP. This abrupt event likely correlates with an abrupt shift in titanium observed in the Cariaco Basin [44], and possibly correlates with the beginning of Event 2 in ocean cores from the North Atlantic [2]. The stepwise decrease in Asian monsoon intensity in the mid–late Holocene suggests the possibility of threshold effects. Variation in $\delta^{18}O$ of 0.5 to 1‰ is spaced throughout the Holocene with some similarities to centennial-scale events seen in other Holocene records [2,6,44]. It is important to note that the magnitude of some of these $\delta^{18}O$ changes in the Holocene is almost half the amplitude of the glacial interstadial events seen in the last glacial period, which would indicate that significant climate variability characterizes the Holocene monsoon.

The record of the Holocene from Dongge Cave is similar to other Holocene records collected from other tropical and subtropical locations. Overall, there is a close correspondence between the Indian monsoon record obtained from stalagmite Q5 from Oman [6] and the monsoon record from D4. Both records show monsoon intensity generally following changes in solar insolation with periods of lighter $\delta^{18}O$ values representing high monsoon intensity. Missing time in Q5 coincides with a period of minimum monsoon intensity in D4 and suggests that a threshold level of monsoon strength was required for stalagmite growth to occur in Oman. In addition, two heavy shifts in $\delta^{18}O$ values ~9.2 ka and ~8.2 ka occur in both records. In Q5, a small (~0.5‰), period of heavy $\delta^{18}O$ values occurs between 8.6 ka and 8.2 ka, while D4 records two brief deviations at ~8.1/8.2 ka. Some minor differences exist such as the sharp shift in $\delta^{18}O$ of D4 at ~3.5 ka, which is not observed in the Q5 record. These differences would suggest that the Indian monsoon in Oman behaves somewhat differently than the monsoon recorded in China, possibly due to different moisture source regions (all Indian Ocean versus Indian and Pacific Ocean sources). However for most of the Holocene, distinct correlations exist.

D4 and the bulk titanium data from the Cariaco Basin [44] bear a remarkable resemblance throughout the Holocene (Fig. 8). Variations are decadal- to centennial-scale in both records and features are similar even in the details. From ~4 ka to 2 ka, high

amplitude variations exist in both records which could be related to increased El Niño-Southern Oscillation (ENSO) variability [44]. These two records most likely are connected as they both represent some manifestation of the intertropical convergence zone (ITCZ). The ITCZ directly controls the location of precipitation over the South American continent and changes in its position affect how much rainfall occurs and therefore the degree of river runoff (as inferred from percent Ti in Cariaco sediments) from northern South America. The ITCZ has a similar effect in China whereby the monsoon front, and therefore precipitation, can be considered a manifestation of the ITCZ [45].

The monsoon record from Dongge Cave as well as those records mentioned above document significant Holocene climate variability at centennial-scales. Other records from the Holocene also show more long-term variability [2] similar to that which is observed during the last glacial period [1]. However, spectral analysis of stalagmite D4 does not show significant power at millennial frequencies. Despite this absence, it is plausible that several of the extreme lows in our monsoon record correlate with North Atlantic ice-rafting events [2], with the best example being the correlation between ice-rafting Event 2 and the weak monsoon immediately after the 3.5 ka abrupt drop. The amount of snow cover on the Tibetan Plateau has been associated with variations in monsoon intensity [46]. Changes in the strength of Eurasian winters related to periods of changing North Atlantic Deep Water formation have the potential to affect snowfall over the Plateau, which ultimately could be responsible for the link between the North Atlantic ice-rafting events and changes in monsoon intensity [5,6]. Plausibly only the largest ice-rafted events triggered an observable response in China.

The results from D4 suggest similar changes in the monsoon between Hulu Cave and Dongge Cave throughout the last deglacial period. This would suggest that changes in the monsoon over this region of China were synchronous over this period. In addition, the Holocene monsoon record from D4 correlates to monsoon changes in Oman as well as the hydrological changes in South America suggesting further synchronicity between the larger Asian monsoon system and climate at other tropical and subtropical localities. These observations do not support earlier work suggesting spatially asynchronous changes in the monsoon over China [47,48]. However, the low density of our sites in China is insufficient to definitively address this issue. Thus, the resolution of this question must await further study.

Solar forcing is a mechanism that has been used to explain centennial- and shorter-scale variation observed in climate records. A common proxy for measuring changes in solar activity is ^{14}C. ^{14}C is produced in the upper atmosphere and its production is related to how much magnetic shielding the Earth experiences. During periods of lowered sunspot activity, solar wind intensity is reduced, which increases the influx of galactic cosmic rays. A higher influx of cosmic rays increases the production of ^{14}C in the atmosphere. The reverse is true during periods of increased sunspot activity when less ^{14}C is produced. Therefore, changes in atmospheric $\Delta^{14}C$ can be related to changes in solar activity. Damon and Peristyhk [49] present results of the Fourier spectral analysis of detrended decadal [50] and single-year [51] $\Delta^{14}C$ data. Several periodicities are present and have been interpreted in terms of solar activity including: (1) the 207-yr De Vries frequency, (2) the 88-yr Gleissberg frequency, and (3) the 10.4-yr Schwabe sunspot cycle.

Bond et al. [2] suggest that the ^{14}C record and the millennial events seen in North Atlantic sediment cores are related. The cores were correlated with the $\Delta^{14}C$ record and explained in large part by a solar forcing mechanism. Spectral analyses on Oman speleothems from the early to middle Holocene [5,6] yield spectral peaks at solar frequencies seen in the $\Delta^{14}C$ record of tree rings [52], thereby linking variations in the Indian monsoon to solar activity.

Spectral analysis of D4 also shows that solar output plays a role in controlling the monsoon and we see this when we statistically compare it to the $\Delta^{14}C$ record. If we consider spectral analysis of the full record, two solar cycles (207 and 88 yr) observed in the $\Delta^{14}C$ record are similar to two cycles seen in the $\delta^{18}O$ record from Dongge cave (208 and 86 yr). If we analyze only the Holocene portion of the record, two similar cycles (217 and 85 yr) are present. Considering the high-resolution portion of the record from 100 to 400 yr we observe a periodicity at 11.6 yr, which is similar to the $\Delta^{14}C$ periodicity of 10.4 yr. The three

corresponding periodicities of 207, 88 and 11.6 years were also observed in the monsoon record from Oman [5,6] demonstrating that solar forcing is an important control on monsoon intensity for a large part of the Asian monsoon system. However, the D4 monsoon spectrum has many other periodicities which do not correspond to solar frequencies, indicating other controls of monsoon intensity.

The modern Asian monsoon shows a strong biennial oscillation between periods of strong and weak monsoons which is an active part of the tropospheric biennial oscillation (TBO) [53,54]. This distinctive periodicity (2–3 yr), which has been observed in the mid-Holocene [19], is contained in the spectral analysis results of the high-resolution portion of D4 from 8110 to 8250 yr BP (2.3 yr). This would suggest that mechanisms causing the oscillation in the modern monsoon were in place as early as 8 ka.

It is likely that other controls of monsoon intensity are broadly related to changes on oceanic and atmospheric circulation. A specific example of this broad type of control is El Niño-Southern Oscillation (ENSO) [55]. The ENSO phenomenon results from a coupling of oceanic and atmospheric processes and creates a distinct pattern of anomalies in the Pacific basin on interannual time scales. Since part of the Asian monsoon originates from the Western Pacific, it is likely that ENSO affects the monsoon. The spectral peaks from the high resolution $\delta^{18}O$ record between 8110 yr and 8250 yr show a number of signature periodicities between 2 and 8 yr (Fig. 7C) which correlate with past and present El Niño periodicities [56,57]. This suggests that ENSO influences the monsoon and that changes in ENSO [44] could be responsible for some of the monsoon variability observed in the Holocene.

6. Conclusions

The Dongge Cave stalagmite record demonstrates that Asian monsoon intensity generally follows changes in insolation and that the response is similar for a large area of China. The mid–late Holocene step-wise decreases in Asian monsoon intensity as well as the presence of centennial-scale events throughout the record demonstrate the variability of the monsoon and its ability to shift abruptly. The centennial- and shorter-scale amplitude of variation is 0.5 to 1‰, up to half of a last glacial period interstadial event as observed in the Asian monsoon [30]. Multiple $\delta^{18}O$ events greater than 1‰ (11.2 ka, 10.9 ka, 9.2 ka, and 8.2 ka) show similarities with changes in the North Atlantic region, possibly related to outburst events from glacial Lake Agassiz. Therefore, the relationship between Greenland and the Asian monsoon, which was observed during the last glacial period, appears to be maintained into the earliest millennia of the Holocene.

Throughout the Holocene, the Asian monsoon exhibits variability, which is highly correlated with other northern low-latitude records. This correlation signifies strong ties between the Asian monsoon and these regions. Asian monsoon intensity and South American hydrological changes show a very strong correlation and are related by changes in ITCZ position. We have clear evidence that some of the variability in the monsoon can be explained by solar variability, as we find significant power at DeVries, Gleissburg, and Schwabe periodicities. However, additional features besides insolation and solar variations must also affect the monsoon as there is significant spectral power at numerous sub-decadal- to multi-century-scale “non-solar frequencies”. It is likely that these periodicities are broadly related to changes in ocean and atmosphere circulations with ENSO being an example of one such phenomenon. In addition, a strong biennial oscillation is observed in the monsoon as early as ~8 ka, suggesting the mechanism was in place during the early Holocene.

Acknowledgements

We are grateful to G. Comer and W. Broecker for their generous support of our work and Broecker’s suggestion of possible links to outflow events. Financial support for this research was funded by NSF grants ESH0214041 and MRI0116395; a Gary Comer Science and Education Foundation Grant (CC8); the National Science Foundation of China grants 40328005 and 40231008; and grants from the Ministry of Land and Resources and the Ministry of Science and Technology of China.

Appendix A. Supplementary data

Supplementary data associated with this article can be found, in the online version, at doi:10.1016/j.epsl.2005.01.036.

References

[1] P. Grootes, M. Stuiver, Oxygen 18/16 variability in Greenland snow and ice with 10^3- to 10^5-year time resolution, J. Geophys. Res. 102 (C12) (1997) 26455–26470.

[2] G. Bond, B. Kromer, J. Beer, R. Muscheler, M.N. Evans, W. Showers, S. Hoffmann, R. Lotti-Bond, I. Hajdas, G. Bonani, Persistent solar influence on North Atlantic climate during the Holocene, Science 294 (2001) 2130–2136.

[3] P. deMenocal, J. Ortiz, T. Guilderson, M. Sarnthein, Coherent high- and low-latitude climate variability during the Holocene warm period, Science 288 (2000) 2198–2202.

[4] J.H. Yin, D.S. Battisti, The importance of tropical sea surface temperature patterns in simulations of Last Glacial Maximum climate, J. Climate 14 (2000) 565–581.

[5] U. Neff, S.J. Burns, A. Mangini, M. Mudelsee, D. Fleitmann, A. Matter, Strong coherence between solar variability and the monsoon in Oman between 9 and 6 kyr ago, Nature 411 (2001) 290–293.

[6] D. Fleitmann, S.J. Burns, M. Mudelsee, U. Neff, J. Kramers, A. Mangini, A. Matter, Holocene forcing of the Indian Monsoon recorded in a stalagmite from southern Oman, Science 300 (2003) 1737–1739.

[7] R.L. Edwards, J.H. Chen, G.J. Wasserburg, ^{238}U–^{234}U–^{230}Th–^{232}Th systematics and the precise measurement of time over the past 500,000 years, Earth Planet. Sci. Lett. 81 (1987) 175–192.

[8] Y.J. Wang, H. Cheng, R.L. Edwards, Z.S. An, J.Y. Wu, C.C. Shen, J.A. Dorale, A high resolution absolute-dated late Pleistocene monsoon record from Hulu Cave, China, Science 294 (2001) 2345–2348.

[9] W. Dansgaard, S.J. Johnsen, H.B. Clausen, D. Dahl-Jensen, N.S. Gundestrup, C.U. Hammer, C.S. Hvidberg, J.P. Steffensen, A.E. Sveinbjornsdottir, J. Jouzel, G. Bond, Evidence for general instability of past climate from a 250-kyr ice-core record, Nature 364 (1993) 218–220.

[10] W.S. Broecker, Massive iceberg discharges as triggers for global climate change, Nature 372 (6505) (1994) 421–424.

[11] Y.H. Ding, C.Y. Li, Y.J. Liu, Overview of the South China sea monsoon experiment, Adv. Atmos. Sci. 21 (3) (2004) 343–360.

[12] D. Yuan, H. Cheng, R.L. Edwards, C.A. Dykoski, M.J. Kelly, M. Zhang, J. Qing, Y. Lin, Y.J. Wang, J.Y. Wu, J.A. Dorale, Z.S. An, Y.J. Cai, Timing, duration, and transitions of the Last Interglacial Asian monsoon, Science 304 (2004) 575–578.

[13] M.J. Kelly, R.L. Edwards, H. Cheng, D. Yuan, Y.J. Cai, M. Zhang, Y. Lin, Z.S. An, High resolution characterization of the Asian monsoon climate during MIS 5 and 6, Palaeogeogr. Palaeoclimatol. Palaeoecol. (submitted for publication).

[14] J.A. Dorale, R.L. Edwards, E.C. Alexander Jr., C.C. Shen, D.A. Richards, H. Cheng, Uranium-series Dating of Speleothems: Current Techniques, Limits, and Applications, Kluwer Academic/Plenum, New York, 2001.

[15] C.C. Shen, R.L. Edwards, H. Cheng, J.A. Dorale, R.B. Thomas, S.B. Moran, S.E. Weinstein, H.N. Edmonds, Uranium and thorium isotopic concentration measurements by magnetic sector inductively coupled plasma mass spectrometry, Chem. Geol. 185 (2002) 165–178.

[16] J.A. Dorale, R.L. Edwards, E. Ito, L.A. Gonzalez, Climate and vegetation history of the midcontinent from 75–25 ka: a speleothem record from Crevice Cave, Missouri, USA, Science 282 (1998) 1871–1874.

[17] C.H. Hendy, The isotopic geochemistry of speleothems—I. The calculation of the effects of different modes of formation on the isotopic composition of speleothems and their applicability as palaeoclimatic indicators, Geochim. Cosmochim. Acta 35 (1971) 801–824.

[18] I. Friedman, J.R. O'Neil, in: M. Fleischer (Ed.), Data of Geochemistry, U.S. Geological Survey Professional Paper, 440-KK, 1977.

[19] D. Sun, M. Gagan, H. Cheng, H. Scott-Gagan, C.A. Dykoski, R. Su, R.L. Edwards, Seasonal and interannual variability of the mid-Holocene East Asian monsoon in coral δ^{18}O records from the South China Sea, Earth Planet. Sci. Lett. (submitted for publication).

[20] D.P. Schrag, G. Hampt, D. Murray, Pore fluid constraints on the temperature and oxygen isotopic composition of the glacial ocean, Science 272 (5270) (1996) 1930–1932.

[21] R.G. Fairbanks, A 17,000-year glacio-eustatic sea-level record: influence of glacial melting rates on the Younger Dryas event and deep-ocean circulation, Nature 342 (1989) 637–642.

[22] E. Bard, B. Hamelin, M. Arnold, L. Montaggioni, G. Cabioch, G. Faure, F. Rougerie, Deglacial sea-level record from Tahiti corals and the timing of global meltwater discharge, Nature 382 (1996) 241–244.

[23] R.L. Edwards, C.D. Gallup, H. Cheng, Uranium-series dating of marine and lacustrine carbonates, in: B. Bourdon, G.M. Henderson, C.C. Lundstrom, S.P. Turner (Eds.), Uranium-series Geochemistry, vol. 52, Mineralogical Society of America, Washington, DC, 2003, pp. 364–405.

[24] R. Gomez, L.A. Gonzalez, H. Cheng, R.L. Edwards, F. Urbani, GSA Abstracts with Programs, Seattle Annual Meeting, 2003.

[25] M. Bar-Matthews, A. Ayalon, M. Gilmour, A. Matthews, C.J. Hawkesworth, Sea–land oxygen isotopic relationships from planktonic foraminifera and speleothems in the Eastern Mediterranean region and their implication for paleorainfall during interglacial intervals, Geochim. Cosmochim. Acta 67 (2003) 3181–3199.

[26] W. Dansgaard, Stable isotopes in precipitation, Tellus 16 (1964) 436–468.

[27] J.M. Lees, J. Park, Multiple-taper spectral analysis: a stand-alone C-subroutine, Comput. Geosci. 21 (1995) 199–236.

[28] S. Bjorck, B. Kromer, S. Johnsen, O. Bennike, D. Hammarlund, G. Lemdahl, G. Possnert, T.L. Rasmussen, B. Wohlfarth, C.U. Hammer, M. Spurk, Synchronized terrestrial-atmospheric deglacial records from around the North Atlantic, Science 274 (5290) (1996) 1155–1160.
[29] D.A. Meese, A.J. Gow, R.B. Alley, G.A. Zielinski, P. Grootes, M. Ram, K.C. Taylor, P.A. Mayewski, J.F. Bolzan, The Greenland ice sheet project 2 depth-age scale: methods and results, J. Geophys. Res. 102 (C12) (1997) 26411–26423.
[30] GISP2, The Greenland Summit Ice Cores, National Snow and Ice Data Center, University of Colorado at Boulder, and the World Data Center-A for Paleoclimatology, National Geophysical Data Center, Boulder Colorado, 1997. (CD-ROM).
[31] S. Johnsen, D. Dahl-Jensen, N.S. Gundestrup, J.P. Steffensen, H.B. Clausen, H. Miller, V. Masson-Delmotte, A.E. Sveinbjornsdottir, J. White, Oxygen isotope and palaeotemperature records from six Greenland ice-core stations: camp century, Dye-3, GRIP, GISP2, Renland and NorthGRIP, J. Quat. Sci. 16 (4) (2001) 299–307.
[32] J.T. Teller, D.W. Leverington, Glacial Lake Agassiz: a 5000 yr history of change and its relationship to the 18O record of Greenland, Geol. Soc. Amer. Bull. 116 (2004) 729–742.
[33] J.T. Teller, D.W. Leverington, J.D. Mann, Freshwater outbursts to the oceans from glacial Lake Agassiz and their role in climate change during the last deglaciation, Quat. Sci. Rev. 21 (2002) 879–887.
[34] W.S. Broecker, Salinity history of the Northern Atlantic during the last deglaciation, Paleoceanography 5 (4) (1990) 459–467.
[35] W.S. Broecker, G. Bond, M. Klas, G. Bonani, W. Wolfli, A salt oscillator in the glacial Atlantic: 1. The concept, Paleoceanography 5 (4) (1990) 469–477.
[36] J.E. Kutzbach, Monsoon climate of the early Holocene: climate experiment with the Earth's orbital parameters for 9000 years ago, Science 214 (1981) 59–61.
[37] S. Clemens, W. Prell, D. Murray, G. Shimmield, G. Weedon, Forcing mechanisms of the Indian Ocean monsoon, Nature 353 (6346) (1991) 720–725.
[38] M. Cohmap, Climatic changes of the last 18,000 years: observations and model simulations, Science 241 (4869) (1988) 1043–1052.
[39] J.E. Kutzbach, Z. Liu, Response of the African monsoon to orbital forcing ocean feedbacks in the middle Holocene, Science 278 (5337) (1997) 440–443.
[40] J. Overpeck, D. Anderson, S. Trumbore, W. Prell, The southwest Indian Monsoon over the last 18,000 years, Clim. Dyn. 12 (3) (1996) 213–225.
[41] K. Wei, F. Gasse, Oxygen isotopes in lacustrine carbonates of West China revisited: implications for post glacial changes in summer monsoon circulation, Quat. Sci. Rev. 18 (2) (1999) 1315–1334.
[42] P. deMenocal, J. Ortiz, T. Guilderson, J. Adkins, M. Sarnthein, L. Baker, M. Yarusinsky, Abrupt onset and termination of the African humid period: rapid climate responses to gradual insolation forcing, Quat. Sci. Rev. 19 (2000) 347–361.
[43] C. Morrill, J. Overpeck, J.E. Cole, A synthesis of abrupt changes in the Asian summer monsoon since the last deglaciation, Holocene 13 (4) (2003) 465–476.
[44] G.H. Haug, K.A. Hughen, D.M. Sigman, L.C. Peterson, U. Rohl, Southward migration of the intertropical convergence zone through the Holocene, Science 293 (2001) 1304–1308.
[45] S. Gadgil, The Indian monsoon and its variability, Annu. Rev. Earth Planet. Sci. 31 (2003) 429–467.
[46] G.A. Meehl, Influence of the land surface in the Asian summer monsoon: external conditions versus internal feedbacks, J. Climate 7 (7) (1994) 1033–1049.
[47] Z.S. An, S.C. Porter, J.E. Kutzbach, W. Xihao, W. Suming, L. Xiaodong, Z. Weijian, Asychronous Holocene optimum of the East Asian monsoon, Quat. Sci. Rev. 19 (8) (2000) 743–762.
[48] Y. He, W.H. Theakstone, Z. Zhonglin, Z. Dian, Y. Tandong, C. Tuo, S. Yongping, P. Hongxi, Asynchronous Holocene climatic change across China, Quat. Res. 61 (2004) 52–63.
[49] P.E. Damon, A.N. Peristykh, Radiocarbon calibration and application to geophysics, solar physics, and astrophysics, Radiocarbon 42 (1) (2000) 137–150.
[50] M. Stuiver, P.J. Reimer, E. Bard, J.W. Beck, G.S. Burr, K.A. Hughen, B. Kromer, G. McCormac, J. Van Der Plicht, M. Spurk, INTCAL98 radiocarbon age calibration, 24,000-0 cal BP, Radiocarbon 40 (3) (1998) 1041–1083.
[51] P.E. Damon, C.J. Eastoe, M.K. Hughes, R.M. Kalin, A. Long, A.N. Peristykh, Secular variation of D14C during the Medieval Solar Maximum: a progress report, Radiocarbon 40 (1) (1998) 343–350.
[52] M. Stuiver, T.F. Braziunas, Sun, ocean, climate and atmospheric $^{14}CO_2$: an evaluation of causal and spectral relationships, Holocene 3 (1993) 289–305.
[53] K.M. Kim, K.M. Lau, Dynamics of monsoon-induced biennial variability in ENSO, Geophys. Res. Lett. 28 (2001) 315–318.
[54] G.A. Meehl, The South Asian monsoon and the tropospheric biennial oscillation, J. Climate 10 (1997) 1921–1943.
[55] M.A. Cane, El Nino, Annu. Rev. Earth Planet. Sci. 14 (1986) 43–70.
[56] D.T. Rodbell, G.O. Seltzer, D.M. Anderson, M.B. Abbott, D.B. Enfield, J.H. Newman, An ~15,000-year record of El Nino-driven alluviation in southwestern Ecuador, Science 283 (1999) 516–520.
[57] K.E. Trenberth, The definition of El Nino, Bull. Am. Meteorol. Soc. 78 (1997) 2771–2777.